Brain Topogr
DOI 10.1007/s10548-013-0277-y

ORIGINAL PAPER

Modulation of EEG Functional Connectivity Networks in Subjects Undergoing Repetitive Transcranial Magnetic Stimulation

Mouhsin M. Shafi · M. Brandon Westover · Lindsay Oberman · Sydney S. Cash · Alvaro Pascual-Leone

Received: 6 September 2012 / Accepted: 20 February 2013

Abstract Transcranial magnetic stimulation (TMS) is a noninvasive brain stimulation technique that utilizes magnetic fluxes to alter cortical activity. Continuous theta-burst repetitive TMS (cTBS) results in long-lasting decreases in indices of cortical excitability, and alterations in performance of behavioral tasks. We investigated the effects of cTBS on cortical function via functional connectivity and graph theoretical analysis of EEG data. Thirty-one channel resting-state EEG recordings were obtained before and after 40 s of cTBS stimulation to the left primary motor cortex. Functional connectivity between nodes was assessed in multiple frequency bands using lagged max-covariance, and subsequently thresholded to construct undirected graphs. After cTBS, we find widespread decreases in functional connectivity in the alpha band. There are also simultaneous increases in functional connectivity in the high-beta bands, especially amongst anterior and interhemispheric connections. The analysis of the undirected graphs reveals that interhemispheric and inter-regional connections are more likely to be modulated after cTBS than local connections. There is also a shift in the topology of network connectivity, with an increase in the clustering coefficient after cTBS in the beta bands, and a decrease in clustering and increase in path length in the alpha band, with the alpha-band connectivity primarily decreased near the site of stimulation. cTBS produces widespread alterations in cortical functional connectivity, with resulting shifts in cortical network topology.

Keywords TMS · EEG · Resting state · Networks · Functional connectivity · Graph theory

Introduction

Transcranial magnetic stimulation (TMS) is a noninvasive brain stimulation method that utilizes electromagnetic induction to produce targeted, transient alterations of cortical physiologic function (Barker et al. 1985; Wagner et al. 2007). During TMS, a large but spatially restricted magnetic flux is used to induce an electrical field in a target cortical area. The induced currents can depolarize neurons

Mouhsin M. Shafi and M. Brandon Westover contributed equally to this study.

Electronic supplementary material The online version of this article (doi:10.1007/s10548-013-0277-y) contains supplementary material, which is available to authorized users.

M. M. Shafi (✉) · M. Brandon Westover · L. Oberman · A. Pascual-Leone
Berenson-Allen Center for Noninvasive Brain Stimulation, Division of Cognitive Neurology, Department of Neurology, Beth Israel Deaconess Medical Center, 330 Brookline Ave, Boston, MA 02215, USA
e-mail: mouhsin.shafi@gmail.com

M. M. Shafi
Epilepsy Service, Department of Neurology, Beth Israel Deaconess Medical Center, West/Baker 5, Boston, MA 02215, USA

M. M. Shafi · M. Brandon Westover · S. S. Cash · A. Pascual-Leone
Department of Neurology, Harvard Medical School, Boston, MA, USA

M. Brandon Westover · S. S. Cash
Epilepsy Service, Department of Neurology, Massachusetts General Hospital, Wang 720, Boston, MA 02114, USA

A. Pascual-Leone
Institut Universitari de Neurorehabilitacio′ Guttmann, Universidad Autónoma de Barcelona, Badalona, Spain

Published online: 08 March 2013

to alter neuronal firing patterns, with neurostimulatory or neuromodulatory effects.

When a train of TMS stimuli is applied (repetitive TMS, or rTMS), changes in cortical activity can persist long after the end of stimulation (Chen et al. 1997; Pascual-Leone et al. 1994; Thut and Pascual-Leone 2010). Huang et al. (2005) recently developed a patterned rTMS protocol in which a "theta-burst" stimulation was used to induce long-term changes in cortical excitability. In the continuous theta-burst stimulation TMS protocol (cTBS), a 40-seconds train of uninterrupted theta-burst stimulation applied to motor cortex resulted in over a 40 % decrease in the amplitude of subsequent motor evoked potentials, with suppression persisting for as long as 60 min. The changes in cortical excitability induced by rTMS are believed to be mediated through stimulation-induced changes in synaptic efficacy, analogous to the synaptic long-term potentiation and long-term depression seen in animal models (Esser et al. 2006), probably via an NMDA-receptor dependent mechanism (Huang et al. 2007; Stefan et al. 2008; Vlachos et al. 2012). Studies in patients with implanted spinal epidural electrodes have demonstrated that the effects of various rTMS protocols, including cTBS, are primarily mediated by trans-synaptic intracortical pathways (Di Lazzaro et al. 2005). A number of studies have demonstrated that rTMS protocols can alter the activity and function of the targeted region. Furthermore, while the effects of a single session of rTMS are transient, repeated sessions of rTMS can produce larger, more persistent changes in cortical excitability and cortical structure (Maeda et al. 2000; May et al. 2007). The durable effect of repeated sessions of stimulation provides the rationale for the therapeutic use of TMS in neuropsychiatric disease.

Single-pulse TMS and rTMS protocols have been applied in a wide variety of experimental settings to explore the cortical mechanisms underlying human behavior. Both single-pulse and repetitive TMS were initially used primarily in a "virtual lesion" mode, to down-modulate the activity of a specific target region, and thereby assess its involvement in various cortical functions(Walsh and Pascual-Leone 2005). For example, inhibitory rTMS applied to the right posterior parietal region has been shown to decrease attention to contralateral space in normal subjects (Hilgetag et al. 2001), thereby providing support for the hypothesis that damage to this region is responsible for the spatial neglect seen in patients with strokes in this region.

More recently, however, studies combining TMS with EEG, PET and fMRI have demonstrated that TMS produces distributed changes in brain activity. For example, single-pulse TMS to the motor cortex produces immediate EEG changes in the region under the TMS coil, which spread over a few milliseconds to ipsilateral motor, premotor and parietal regions, and then several milliseconds later to the contralateral motor cortex (Ilmoniemi et al. 1997; Komssi et al. 2002). In one recent study, stimulation of different regions within visual cortex resulted in widespread, long-lasting oscillations, with the precise pattern of network activations containing both stimulation site-specific and site-invariant features (Garcia et al. 2011). Similarly, a number of studies have demonstrated that rTMS produces alterations in activity in distributed networks. One seminal early study (Paus et al. 1997) demonstrated that when rTMS trains were applied to the left frontal eye field, correlated changes in blood flow occurred both locally and in several other distant functionally connected regions, including the left medial parieto-occipital cortex, the bilateral superior parietal cortex, and the right supplementary eye fields. Studies using EEG functional connectivity measures such as coherence have provided evidence that rTMS can alter the strength of connections between different cortical regions (Jing and Takigawa 2000; Plewnia et al. 2008).

Such network effects may play an important role in the efficacy of rTMS in inducing behavioral changes. For example, inhibitory rTMS has been applied to the contralesional cortex to improve motor function in stroke patients (Khedr et al. 2009). fMRI functional connectivity studies have shown that inhibitory rTMS to contralesional motor cortex results in *decreased* pathologic inhibitory coupling from contralesional to ipsilesional motor cortex, as well as a *increased* ipsilesional SMA-M1 coupling; the decrease in the pathologic inhibitory coupling from contralesional to ipsilesional motor cortex is correlated with the observed improvement in motor function (Grefkes et al. 2010). Another recent study found that the reported antidepressant efficacy of rTMS of different prefrontal sites is related to the functional connectivity of each site with the subgenual cingulate cortex (Fox et al. 2012), suggesting that successful rTMS therapy is dependent on modulation of the entire network rather than just a local prefrontal region. Thus, an appreciation of the network effects of focally applied TMS can provide critical insights into brain function under both normal and pathologic circumstances, identify how rTMS modulates human cognition and behavior, and potentially guide the therapeutic use of rTMS in neuropsychiatric disease (Shafi et al. 2012). In this study, we aim to expand such insights by using graph theory techniques to evaluate the effects of cTBS on EEG functional connectivity networks.

The identification of complex functional connectivity networks in the human brain has led to the use of graph theory techniques in the analysis of network topologies. Mathematically, networks are represented as graphs, which are groups of interacting entities (nodes), connected by lines (edges) indicating which pairs of nodes directly

interact. These nodes can represent neurons, populations of neurons within different anatomical brain regions, or the locations of sensors which measure neural activity (as in EEG). Certain important generic network properties depend solely on the topological properties of the underlying networks, regardless of the details of the underlying network function. One important property, the clustering coefficient, evaluates the degree of connectivity within local regions. High clustering is associated with local information processing efficiency (Bullmore and Sporns 2009; Latora and Marchiori 2003; Reijneveld et al. 2007). Another important property, path length, describes the average distance between any two nodes of the network, and is inversely related to the global efficiency of information transfer. A number of EEG and MRI studies have applied graph theoretic analyses to human brain networks, and the results support the notion that human brain networks have a "small-world" topology, an architecture with high local and global processing efficiency (Achard and Bullmore 2007; Reijneveld et al. 2007). Alterations of "small-world" network topologies have been implicated in human diseases such as Alzheimers (Stam et al. 2007, 2009), schizoprenia (Rubinov et al. 2009; van den Heuvel et al. 2010) and multiple sclerosis (He et al. 2009; Schoonheim et al. 2011; Shu et al. 2011). More recently, it was shown that facilitatory anodal transcranial direct current stimulation (tDCS) applied to the left primarymotor cortex produced increased EEG synchronization within the left hemisphere, as well as interhemispheric desynchronization in the α, β and high-γ bands (Polanía et al. 2011a). Another study demonstrated increased fMRI resting state functional connectivity after left motor tDCS in distant brain regions, and an increase in mean path length within the stimulated region (Polanía et al. 2011b). Thus, noninvasive brain stimulation may produce widespread changes in the topology of brain functional connectivity.

TMS is currently used in a variety of experimental settings aimed at elucidating the mechanisms of human cortical function, and is also under investigation as a therapeutic tool in a numerous neuropsychiatric diseases. However, to our knowledge, functional connectivity network analysis techniques have not previously been applied to investigate how cTBS alters the topology of human cortical networks. In the present study, we investigate how continuous theta-burst stimulation rTMS, a procedure that typically leads to inhibition of local cortical output, alters network topologies and graph theoretical measures. Continuous theta-burst stimulation was applied to left primary motor cortex, and 31-channel EEG was recorded before and after cTBS, in the resting state. Offline, EEG activity was bandpass filtered to isolate component signals into different frequency bands of physiological interest. Functional connectivity between different surface brain regions ("nodes") was then determined, and the changes in functional connectivity after cTBS were assessed. The resulting network graphs were evaluated for spatial patterns of alterations and for changes in measured graph theoretic parameters.

In keeping with the previous literature (e.g. Jing and Takigawa 2000), we hypothesized that the inhibitory cTBS protocol utilized here would result in decreased functional coupling of the stimulated region with other areas. However, previous literature also suggests that the changes in excitability of the stimulated region may produce widespread alterations in functional connectivity extending beyond the site of stimulation, particularly in other cortical motor network regions (Bestmann et al. 2004); for example, decreased interhemispheric inhibition from the stimulated motor cortex might result in increased functional coupling contralaterally (Grefkes et al. 2010). We further hypothesized that these shifts in functional connectivity would lead to an alteration of network topology, with changes in graph theoretic measures related to local and global information processing. Specifically, increased functional coupling within the motor network might lead to an increase in the clustering coefficient, while disconnection of the stimulated motor region might result in an increase in mean path length.

Materials and Methods

Subjects

The study involved 13 healthy volunteers (4 men and 9 women; mean age, 35.2 $\pm$ 19.8 years; range 20–67 years). All subjects gave informed consent. None of them suffered from any significant neurological disorder, and none had any implanted metallic electrical devices. The experiments conform to the Declaration of Helsinki and were approved by the Human Subjects Institutional Review Board of the Beth-Israel Deaconess Medical Center. All subjects provided informed consent prior to inclusion in the study.

Transcranial Magnetic Stimulation

We applied the continuous TBS paradigm (Huang et al. 2005) as three pulses of 50 Hz stimulation repeated at 200 ms intervals for 40 s (600 pulses), with the stimulus intensity set at 80 % active motor threshold. TMS was delivered using a hand-held figure-eight coil attached to a Magstim Super Rapid stimulator. The coil was placed tangentially to the scalp with the handle pointing posteriorly for all stimulation. All stimulation was applied over the hand area of the left motor cortex and individually localized for each participant based on the optimal position for eliciting MEPs in the right FDI. In order to precisely target the stimulation site (primary motor cortex) and keep

the brain target constant throughout the stimulation session, we used a frameless stereotactic neuronavigation system (Brainsight, Rogue Inc).

Electroencephalography

Figure 1 schematically summarizes all steps of pre- and post-processing. EEGs were recorded while subjects sat in a comfortable reclined chair. EEG was recorded for at least 30 min with the subject in the eyes-closed, awake, resting state, after which the subject received cTBS. Afterwards, an additional 10 min of EEG data was recorded with the subject in the eyes-closed, awake, resting state. We chose to test subjects with eyes closed to reduce the presence of eye movement and muscle artifacts. EEGs were recorded with an AFz reference using a Brainvision Brainamp DC system, with DC amplifiers to minimize the artifact induced by the TMS pulse. EEGs were recorded at the following 31 positions of the international 10–10 system: Fp1, Fp2, F7, F3, Fz, F4, F8, FC5, FC1, FC2, FC6, T7, C5, C3, C1, Cz, C2, C4, T8, CP5, CP1, CP2, CP6, P7, P3, Pz, P4, P8, O1, Oz, and O2. Electrode impedances were kept less than 5 kΩ throughout the experiment. The EEG data was recorded with a sampling frequency at 512 or 1,024 Hz. The EEG data was subsequently processed offline.

Preprocessing

EEG data recorded with a sampling frequency of 1,024 Hz was down-sampled to 512 Hz to match the remaining data. EEG data was subsequently converted to an average reference format. We utilized the following procedure for identifying and rejecting data segments corrupted by artifacts: Low-frequency drifts were removed by first convolving the data in each channel with a broad Gaussian filter with a standard deviation of 2 s and subtracting the result from the raw data. The resulting detrended data was subjected to a semi-automatic artifact rejection procedure involving thresholding the data to highlight and remove high-amplitude artifactual events, eye blinks, and muscle artifact. Continuous segments of 3-seconds duration were identified in this artifact-free data, and these data segments were then bandpass filtered using a finite impulse response filter (EEGLAB (Delorme and Makeig 2004) function eegfilt), with the filter order set to 3 times the sampling rate divided by the lower edge of the frequency passband,to isolate EEG activity within each of the following frequency bands: 4–30 Hz (broad band), 4–8 Hz (theta), 8–13 Hz (alpha), 13–18 Hz (low beta), 18–24 Hz (mid-beta) and 24–30 Hz (high beta). A segment length of 3 s was chosen to ensure accurate bandpass filtering at the lowest analyzed frequency. The subsequent functional connectivity analysis was conducted on these 3-second bandpass filtered data segments.

Functional Connectivity Analysis

Functional connectivity between all pairwise combinations of the 31 EEG channels was computed independently for each 3-second data segment utilizing the Matlab (The Mathworks, Natick, Massachusetts) cross-covariance function *xcov*. The cross-covariance of two sequences x and y at lag m is:

$$c_{xy}(m) = \begin{cases} \sum_{n=0}^{N-|m|-1} \left(x(n+m) - \frac{1}{N}\sum_{i=0}^{N-1} x_i \right) \left(y_n^* - \frac{1}{N}\sum_{i=0}^{N-1} y_i^* \right) & m \geq 0 \\ c_{yx}^*(-m) & m < 0 \end{cases}$$

The cross-covariances were normalized so that the auto-covariances at zero lag are identically equal to 1.0. The functional connectivity value between two electrodes for a given data segment was defined as the maximum cross-covariance (MC) value of the two electrodes, where the maximum is computed by searching over lags (m) of ±300 ms. The mean functional connectivity for each electrode pair (for each frequency band and subject) was then defined for the pre-cTBS and post-cTBS periods by averaging the MC values for all of the 3-second data segments within each time period. We also constructed grand average max-covariance matrices pre- and post-cTBS in each frequency band by averaging (across subjects) the mean functional connectivity value for each electrode pair.

Changes in Functional Connectivity After cTBS

We evaluated for significant changes in functional connectivity (mean MC value) after cTBS for each subject and frequency band. For each individual subject, the non-parametric two-sample Kolmogorov–Smirnov test was used to identify significant changes in the distribution of MC values after cTBS for each electrode pair. A significance threshold of $p < 0.05$ (Bonferroni-adjusted for the total number of connections tested) was applied. For the grand-average functional connectivity data, the paired-sample t test was used to compare the mean of the single-subject max-correlation values for each electrode pair, before and after cTBS, across all subjects using an (uncorrected) significance threshold of $p < 0.0005$. To assess for global effects of cTBS on MC values in each frequency band, a 2-factor ANOVA was performed with frequency band as one factor, period (pre- vs post-cTBS) as the second factor, and the single-subject mean (across electrodes) MC values as the observations.

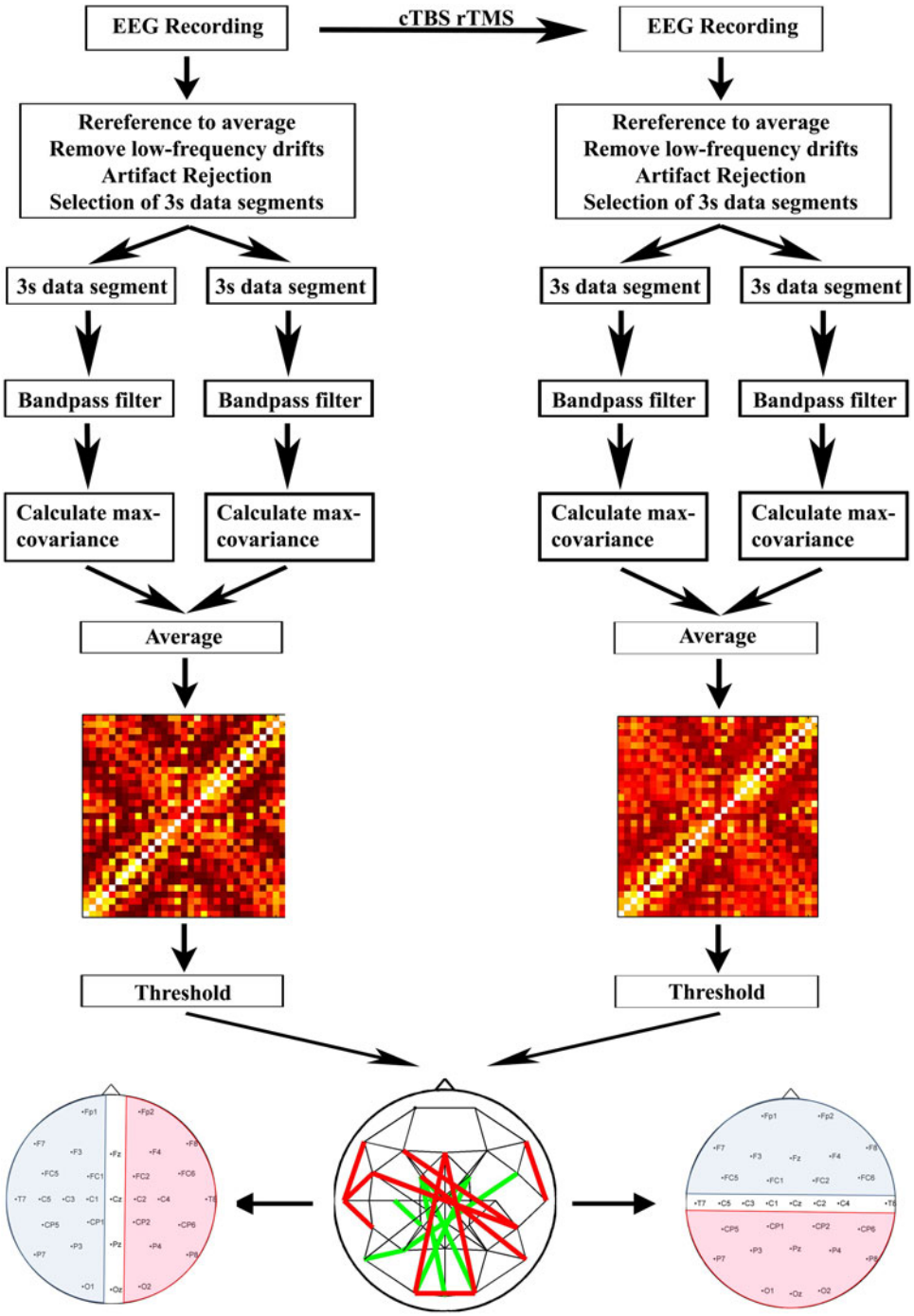

Fig. 1 Experimental setup and data processing for each subject. EEG was recorded for up to 30 min with the subject in the eyes-closed, awake, resting state. This was followed by administration of 40 s of continuous theta burst repetitive TMS (cTBS). Afterwards, an additional 10 min of EEG data was recorded with the subject in the eyes-closed, awake, resting state. The EEG data was subsequently processed offline. The data was downsampled to 512 Hz, re-referenced to an average reference, and then detrended. Segments of data with artifact were subsequently removed, and multiple continuous 3-second segments of artifact-free data identified. Lagged max-covariance (MC) analysis was done on these 3-second segments, then average max-covariance values for each electrode pair were obtained by averaging across the values for individual 3 s segments. Subsequently a MC matrix was built. The MC matrices were thresholded to produce undirected graphs. Electrodes were grouped by hemisphere (*left*; *blue* = *left*, *pink* = *right*, *clear* = *midline*) or anterior–posterior axis (*right*; *blue* = *anterior*, *pink* = *posterior*, *clear* = *midline*)

Anterior–Posterior and Hemispheric Patterns, and Statistical Analysis

To quantitatively examine patterns of changes in functional connectivity after cTBS, we grouped connections along the anterior-posterior and right-left axes, and performed statistical tests on these groups. In the anterior-posterior analysis, the EEG channels were first partitioned into anterior, central or posterior regions. The anterior region consisted of the following channels: Fp1, Fp2, F7, F3, Fz, F4, F8, FC5, FC1, FC2, and FC6. The central region consisted of the following channels: T7, C5, C3, C1, Cz, C2, C4, T8. The posterior region consisted of: CP5, CP1, CP2, CP6, P7, P3, Pz, P4, P8, O1, Oz, O2. If both electrodes were anterior, or if one electrode was anterior and the other was central, then the connection between the two was labeled an "anterior" connection. If both electrodes were posterior, or if one was posterior and the other central,

the connection was labeled a "posterior" connection. Connections where one electrode was from the anterior region and the other was from the posterior region were defined as "interregional." Connections between two central electrodes were ignored during subsequent analyses.

For each subject, we then calculated the percentage of connections changed after cTBS for each connection type (anterior, posterior or interregional) in each frequency band. A 2-factor repeated measures ANOVA (with connection type and frequency band as the two factors, and the percentage of connections changed as the observations) was used to assess for significant main effects and interactions, at a significance threshold of $p < 0.05$. If a significant main effect was identified, post hoc t tests were conducted, and a Bonferroni-adjusted significance threshold of $p < 0.05$ was applied. Similar statistical analyses were conducted with the percentage of connections unchanged after cTBS as the observations, and again with percentage of connections strengthened and percentage of connections weakened. We also calculated a modulation index (percentage of connections changed/percentage of connections present) as well as a strengthening index (percentage of connections strengthened $\times$ 2/percentage of connections changed) for each subject as a function of frequency band and connection type, and a similar statistical analysis was conducted on each of these measures as well.

To analyze within hemisphere changes in connectivity following cTBS, the EEG channels were first partitioned into left hemispheric, right hemispheric and midline subsets according to standard EEG convention (left hemispheric—Fp1, F7, F3, FC5, FC1, T7, C5, C3, C1, CP5, CP1, P7, P3, O1; right hemispheric—Fp2, F8, F4, FC6, FC2, T8, C4, C2, CP6, CP2, P8, P4, O2; midline—Fz, Cz, Oz). If both electrodes were right hemispheric, or if one of the electrodes was right hemispheric and the other was midline, the connection between the two was labeled a "right intrahemispheric" connection. If both electrodes were left hemispheric, or if one electrode was left hemispheric and the other was midline, the connection was labeled a "left intrahemispheric" connection. If one electrode was right hemispheric and the other was left hemispheric, the connection was labeled "interhemispheric." Connections between two midline electrodes were ignored. Subsequent statistical analysis was conducted following the same approach as described above for the connections grouped according to region.

Undirected Graphs

To evaluate changes in network topologies after cTBS, we constructed undirected graphs in both the pre-cTBS and post-cTBS period. For each subject, the mean functional connectivity within each frequency band was calculated for all possible pairwise electrode combinations, resulting in a 31 $\times$ 31 matrix, where each entry N_{ij} contained the mean value (across data segments) of the maximum cross-covariance measured for that electrode pair, MC_{ij}. Then, for each individual data set (and for the grand average across subjects), an undirected graph was constructed consisting of 31 nodes (EEG channels), with the presence or absence of edges (e_{ij}) connecting each node pair determined by applying a threshold T to the max-covariance matrix, such that $e_{ij} = 1$ if $N_{ij} > \mathrm{T}$, and $e_{ij} = 0$ if $N_{ij} \leq \mathrm{T}$. Hence, if the functional connectivity (mean MC value) between two EEG channels i and j was greater than the value T, an edge was defined as being present between them.

In one set of analyses (fixed-density analyses), for each subject (and for the grand average across subjects), the threshold was set independently for the pre-cTBS and post-cTBS periods to produce the same mean connectivity degree in each period (over a range of mean connectivity degrees—see below). As an illustrative example, we set the threshold in both periods to produce networks with a mean connectivity degree of four connections per node in either period. The resulting graphs had exactly 62 connections, (resulting in an average connection density of four connections per node), in both the pre-cTBS and post-cTBS periods for each subject.

In the second set of analyses (variable-density analyses), the threshold was set for each subject to produce a specific mean connectivity degree in the pre-cTBS networks, and then the same threshold was applied to the post-cTBS data. For example, the threshold could be set to produce networks with exactly 62 connections (an average connection density of four connections per node) in the pre-cTBS graphs; the same threshold was then applied to the post-cTBS graphs, which could result in networks with varying numbers of connections.

Both the fixed-density analyses and the variable-density analyses were performed systematically over a range of thresholds, resulting in networks with average connection densities ranging from two connections per node, up to sixteen connections per node. We subsequently evaluated the anterior–posterior and hemispheric patterns of connectivity, analogous to the evaluation of regional and hemispheric changes in connectivity described in the previous section. For both the fixed-density and variable-density networks obtained for each subject at each frequency band and density, connections were defined as "anterior", "posterior", or "interregional" as described in the previous section. We then determined the percent of possible connections present in either period, the percent present but unchanged by cTBS, the percent changed, the modulation index, and the strengthening index for each

connection type. A two-way repeated measures ANOVA was performed in each frequency band, with connection type (anterior, posterior or interregional) as one factor, density as the second factor, and the percent of connections present (or the percent of connections changed, the modulation index, or the strengthening index) as the observed variable. Post-hoc testing of the significance of marginal means was performed using Tukey's HSD, while pairwise comparisons between cell means was performed using paired t tests.

Graph Theory Analysis

The two most commonly evaluated graph theory statistics include the clustering coefficient and path length. The clustering coefficient evaluates the degree of connectivity within local regions; networks with higher clustering are said to have greater local efficiency of information processing and robustness. The path length is a measure of the connectivity distance between all the nodes of a network; in networks with high average path length, the distance between any two nodes (i.e. the number of edges that must be traversed in traveling from node a to node b) is large, and therefore the global efficiency of information processing is low. The graph theory metrics of node degree, clustering coefficient (C) and path length (L) were calculated for the undirected graphs constructed via the methods described above. For each node i, the clustering coefficient C_i assesses the proportion of neighboring vertices (i.e. vertices directly connected to the node in question) that are connected to each other. The value of the clustering coefficient is therefore always between 0 and 1, and the mean clustering coefficient C for a graph is simply the average of the clustering coefficients for all the nodes of that graph. The path length L_{ij} between any two nodes i and j is the distance (the minimum number of edges that must be traversed) from i to j. Conventionally, the mean path length L for a graph is simply the mean of the path lengths between all the nodes of the graph. However, in networks with unconnected nodes, as in this study, the mean path length is infinite.

To avoid this problem, the mean path length L calculated in this study is actually the "harmonic mean", which assigns a value of $+\infty$ to unconnected node pairs, and then calculates the mean path length as follows (Newman 2003):

$$L = \frac{\frac{1}{2}n(n-1)}{\sum_{i=1}^{n-1}\sum_{j=i+1}^{n}\frac{1}{L_{ij}}}$$

The mean clustering coefficient C and mean path length L were determined for each subject in each frequency band at each network density, both pre-cTBS and post-cTBS. For each measure, a 2-factor repeated-measures ANOVA (with pre- versus post-cTBS as one factor, and density as a second factor) was performed in each frequency band to assess for significant main effects, and post hoc testing was performed using paired t tests. We also assessed the node degree for each electrode before and after cTBS for each subject at every network density, in each frequency band. A 2-factor repeated-measures ANOVA (with pre- vs post-cTBS as one factor, density as the second factor, and node degree as the observations) was performed in each frequency band, and nodes that showed a significant main effect of time period (pre- vs post-cTBS) at a significance level of $p < 0.001613$ (Bonferroni adjusted $p < 0.05$ for the 31 electrodes) were identified in each frequency band.

Results

Patterned Network Connectivity Changes After cTBS

A 31 $\times$ 31 channel matrix, consisting of the max-correlation values for each electrode pair, was obtained for each subject before and after cTBS, and significant changes in connectivity were assessed for each subject as described in the methods section above. While there was substantial variability in the specific connectivity changes seen in different subjects, several common patterns were present across subjects. For example, in the broadband (4–30 Hz) frequency range, there was an anterior-predominant strengthening of connectivity after cTBS (Fig. 2). Figure 3a shows the grand average (across all subjects) MC matrices before and after cTBS in the broadband (4–30 Hz) range; connections are ordered based first on hemisphere (all left hemispheric before all right hemispheric), then region (frontal, central or posterior), and finally from lateral to midline (for example, F7 before F3). Some broad patterns are immediately visible, such as an increase in max correlation values between left (1–9) and right (19–26) frontocentral channels. When the connections with significant changes in functional connectivity (unadjusted $p < 0.0005$) after cTBS across all subjects are identified for each frequency band, frequency-specific, region-specific and hemisphere-specific patterns in connectivity changes can be seen (Fig. 3b). There is a widespread decrease in functional connectivity in the alpha band. There is also an increase in functional connectivity in the high-beta and broad bands, most prominent anteriorly. In the theta band, there appears to be an increase in connectivity between anterior interhemispheric connections, with a concomitant decrease in connectivity between posterior, interregional or short-range connections. Interhemispheric connections are more likely to be altered than intrahemispheric connections. These changes are analyzed in further detail below.

Alpha-band Decreases and Beta-band Increases in Functional Connectivity After cTBS

The percent of connections significantly changed for individual subjects after cTBS varies significantly as a function of frequency band ($F(5,60) = 7.0$; $p < 0.001$), as does the percent of connections strengthened ($F(5,60) = 10.8$, $p < 0.001$), the percent of connections weakened ($F(5,60) = 11.3$, $p < 0.001$), and the strengthening index ($F(5,60) = 11.3$, $p < 0.001$). A greater percentage of connections were changed in the alpha band (8–13 Hz) than in the beta bands (13–18, 18–24, and 24–30 Hz), with the least connections changed in the theta (4–8 Hz) frequency band (Fig. 4). When the percentage of connections strengthened after cTBS is evaluated, there is once again a main effect of frequency ($F(5,60) = 10.8$, $p < 0.0001$), with post hoc testing demonstrating significantly (Bonferroni-adjusted $p < 0.05$) more connections increased in the high-beta (24–30 Hz) band than in the low-beta, mid-beta or theta bands (Fig. 4b). There are significantly fewer connections strengthened in the alpha band than in any other frequency band. In comparison, significantly more connections are weakened in the alpha band than in any other frequency band (Fig. 4c). Consequently, the strengthening index (see Materials and Methods for definition) is significantly higher in the high-beta band than in any other frequency band, and is significantly lower in the alpha band (Fig. 4d). In addition, there is also a significant interaction between frequency band and period (pre- vs post-cTBS) for the raw mean (across electrodes) max-correlation values ($F(5,60) = 25.7$, $p < 0.001$). Specifically, there is a significant decrease in mean max-correlation values after cTBS in the alpha band ($p < 0.001$), and a significant increase in mean max-correlation values after cTBS in the high-beta band ($p = 0.027$).

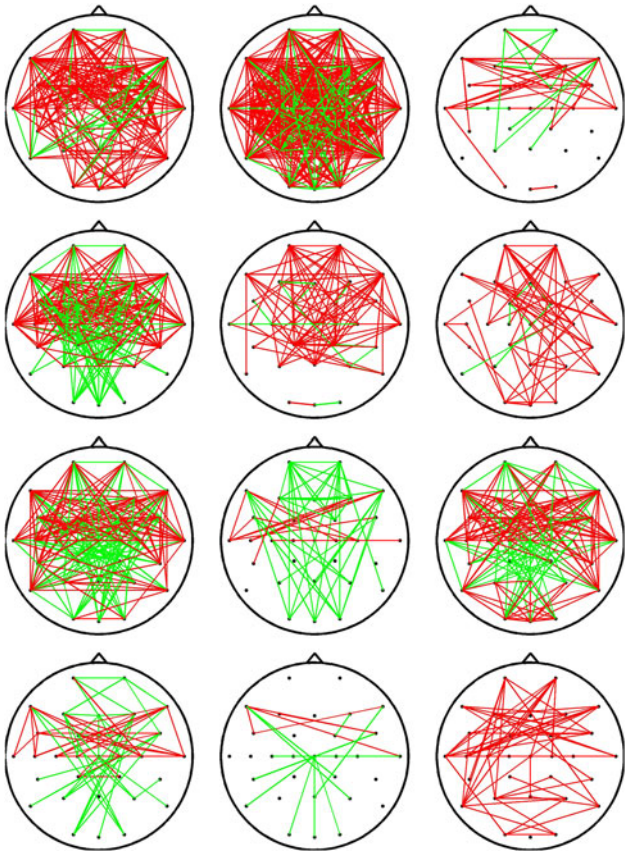

Fig. 2 Functional connectivity changes after cTBS. EEG channels with a significant (Bonferroni adjusted $p < 0.05$) increase (*red*) or decrease (*green*) in functional connectivity, as measured via lagged max-correlation, in the broadband (4–30 Hz) frequency range, for each of the 12 subjects with significant changes in functional connectivity after cTBS (1 subject had no significant changes)

Anterior Connections are Strengthened After cTBS

The percent of connections significantly changed after cTBS varies as a function of region ($F(2,24) = 6.6$; $p = 0.005$), as does the percent of connections strengthened ($F(2,24) = 11.5$, $p < 0.001$), and thus the strengthening index ($F(2,24) = 15.0$, $p < 0.001$). A significantly (Bonferroni-corrected $p < 0.05$) greater percentage of connections within the anterior region are altered after cTBS than for posterior and interregional connections (Fig. 4a); specifically, more of the anterior connections are strengthened than for either the posterior or interregional connections (Fig. 4b). There is no main effect of region for the percent of connections weakened, although on visual inspection fewer connections appear to be weakened in the anterior region than in other regions across frequency bands (Fig. 4c). However, the strengthening index is significantly (Bonferroni-corrected $p < 0.05$) higher for anterior connections than for the posterior or interregional connections (Fig. 4d).

Interhemispheric Connections are Strengthened

A significant main effect of hemispheric connection type is present for the percent of connections significantly changed after cTBS ($F(2,24) = 6.1$, $p = 0.007$), the percent of connections strengthened after cTBS ($F(2,24) = 11.7$, $p < 0.001$), the percent of connections weakened ($F(2,24) = 5.1$, $p = 0.01$), and the strengthening index ($F(2,24) = 8.5$, $p = 0.002$). Significantly more of the interhemispheric connections are altered than within either set of intrahemispheric connections (Bonferroni-corrected $p < 0.05$; Fig. 5a). Specifically, more interhemispheric connections are strengthened (Fig. 5b), and fewer interhemispheric connections are weakened (Fig. 5c). Consequently, the strengthening index is significantly (Bonferroni-corrected $p < 0.05$) higher for the interhemispheric connections than for either the right or the left intrahemispheric connections (Fig. 5d), across all frequency bands.

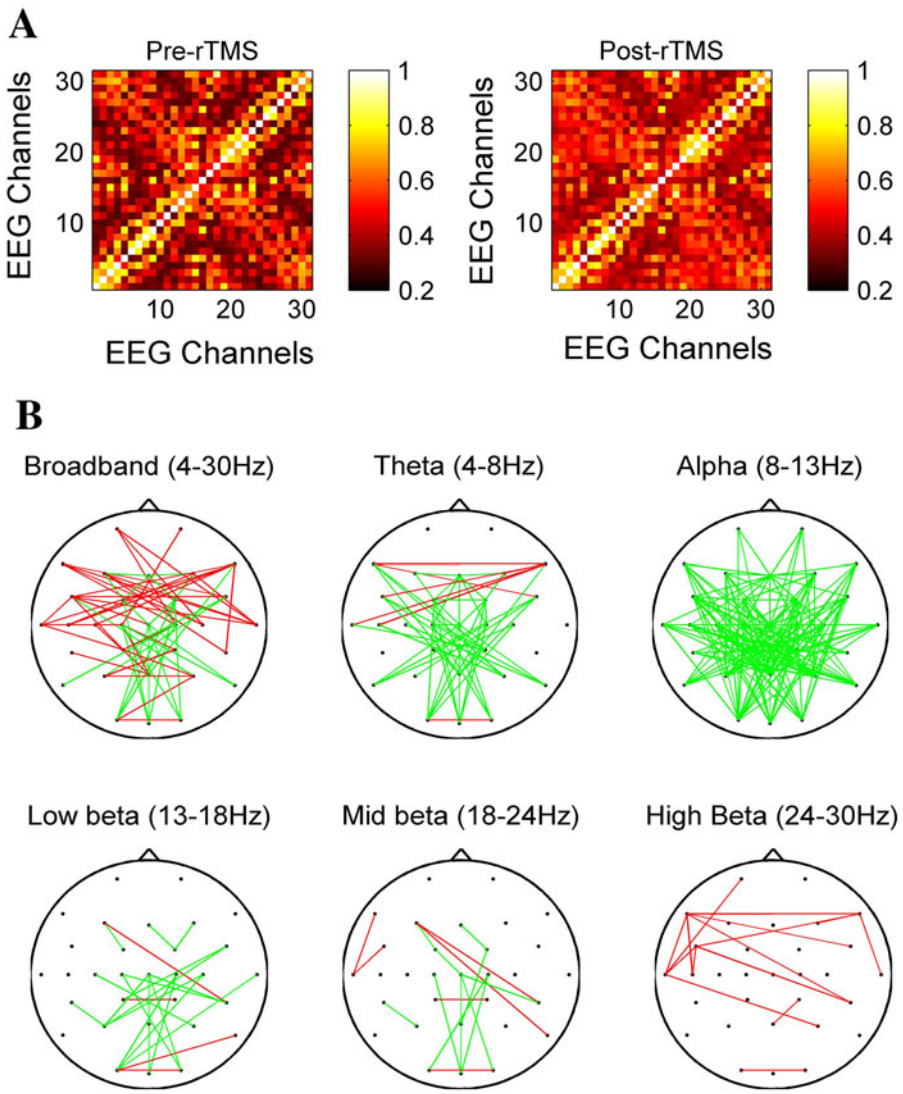

Fig. 3 Max-correlation matrices and average functional connectivity changes. **a** shows the mean max-correlation matrices averaged across all subjects in the 4–30 Hz (broadband) frequency range before (*left*) and after (*right*) cTBS. The order of the electrodes is: Fp1, F7, F3, FC5, FC1, T7, C5, C3, C1, CP5, CP1, P7, P3, O1, Fz, Cz, Pz, Oz, Fp2, F8, F4, FC6, FC2, T8, C4, C2, CP6, CP2, P8, P4, O2. **b** shows the EEG channels with significant (unadjusted $p < 0.0005$) changes in functional connectivity after cTBS, across subjects, in each of the different frequency bands. Connections with increased connectivity are illustrated in *red*, connections with decreased connectivity are drawn in *green*

No Significant Correlation Between Age and cTBS-induced Connectivity Changes

There was no significant correlation between the age of the subjects and the number of connections changed in any frequency band ($r^2 < 0.17$ in all bands; $p > 0.1$ uncorrected in each band). There was also no significant correlation between the age of the subjects and the mean absolute change in connection strength for each subject ($r^2 < 0.10$ in all bands; $p > 0.1$ uncorrected in each band).

cTBS Primarily Modulates Interhemispheric and Anterior/Interregional Connections of Moderate Initial Strength

Undirected graphs were constructed for the EEG data recorded before and after cTBS by applying a threshold T to the maximum cross-covariance values. In the fixed-density networks, the threshold was set independently for the pre-cTBS and post-cTBS data to produce graphs with the same mean connectivity degree in each period; a series of networks were constructed with mean connectivity degrees ranging from 2 to 16. To illustrate, Fig. 6a shows the networks resulting when the thresholds are adjusted to produce networks with a mean connectivity degree of four in each period (i.e. each electrode is connected with four other electrodes, on average). At this connection density, there appears to be a structural core consisting of short-range local intrahemispheric and intraregional connections that is present bilaterally both before and after cTBS, while longer-range interhemispheric and interregional connections are modulated.

The distribution of connections within vs between hemispheres varied as a function of network connection density (Fig. 6b and c). For example, in the broad band, there is a main effect of hemisphere ($F(2,24) = 52.1$, $p < 0.001$) for the percent of stable connections (present both before and aftercTBS), with significantly fewer

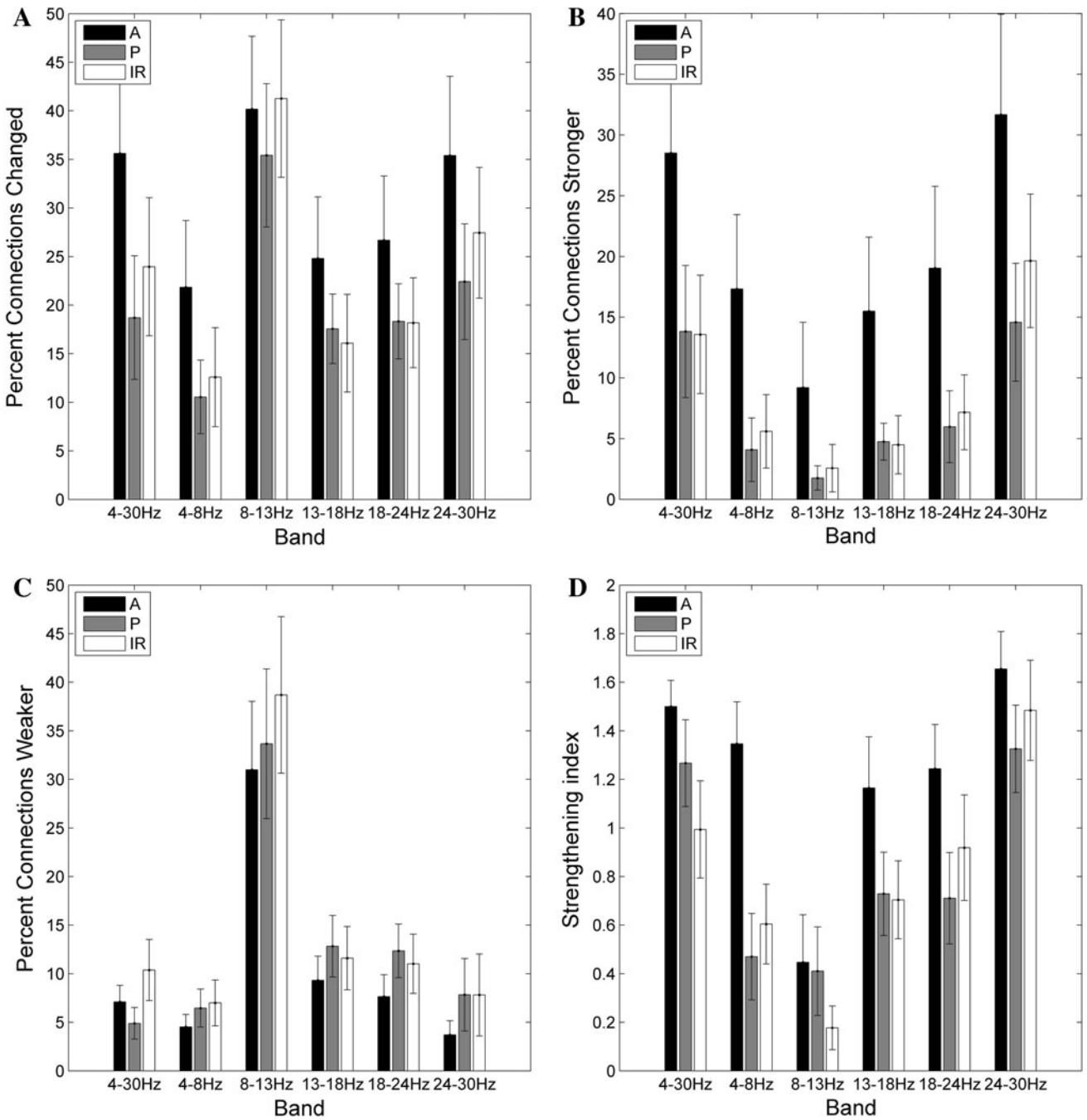

Fig. 4 Frequency and region-specific changes in connection strength. **a** The average (across subjects) percentage of connections significantly changed after cTBS as a function of frequency band and region. **b** The average percentage of connections strengthened after cTBS. **c** The average percentage of connections weakened after cTBS. **d** The strengthening index (percentage of connections strengthened × 2/percentage of connections changed); A value greater than 1 indicates that more connections were strengthened than weakened, whereas a value less than 1 indicates that more connections were weakened. *A* = connection between two anterior electrodes, *P* = connection between two posterior electrodes, *IR* = interregional connection between an anterior and posterior electrode

interhemispheric than left (marginal means 20.0 vs 26.3 %, $p < 0.05$) or right (marginal means 20.0 vs 26.3 %, $p < 0.05$) connections (Fig. 6b). However, there was also a significant interaction between connection density and the hemispheric distribution of stable connections ($F(28,336 = 22.9$; $p < 0.001$), with no significant difference ($p > 0.05$ uncorrected) between the number of interregional versus left or right connections at mean connection densities greater than 13 connections per node. In contrast, when looking at modulation by cTBS, the

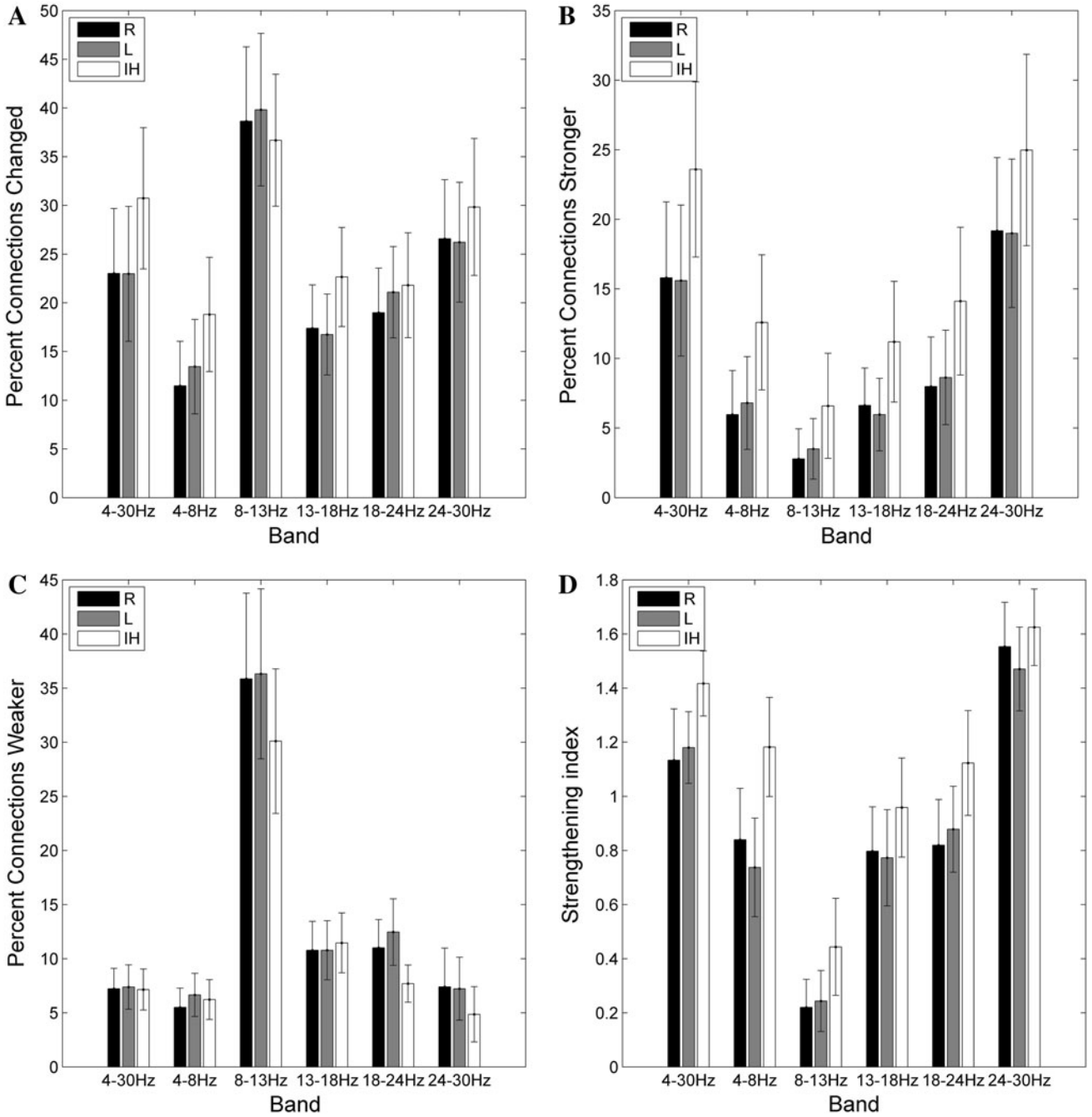

Fig. 5 Frequency and hemisphere-specific changes in connection strength. **a** The average percentage of connections significantly changed after cTBS as a function of frequency band and hemisphere. **b** The average percentage of connections strengthened after cTBS. **c** The average percentage of connections weakened after cTBS. **d** The strengthening index (defined in Fig. 4 legend)

interhemispheric connections are more likely to be modulated by cTBS across connection densities ($F(2,24) = 66.9$; $p < 0.001$) than either the left connections (marginal means 53.9 % modulated vs 29.0 %, $p < 0.05$) or right connections (marginal means 53.9 vs 31.8 %, $p < 0.05$) (Fig. 6C); this difference remained significant at all densities ($p < 0.001$ uncorrected). Taken together, these results suggest that within each hemisphere, there is a population of strong connections, as well as a population of weak connections, while the interhemispheric connections are of moderate strength. The interhemispheric connections are the ones whose presence is most likely to be modulated by cTBS.Similar patterns were seen in other frequency bands (see Supplementary Figs. 1–2).

The distribution of connections within the anterior or posterior regions versus connections that cross from

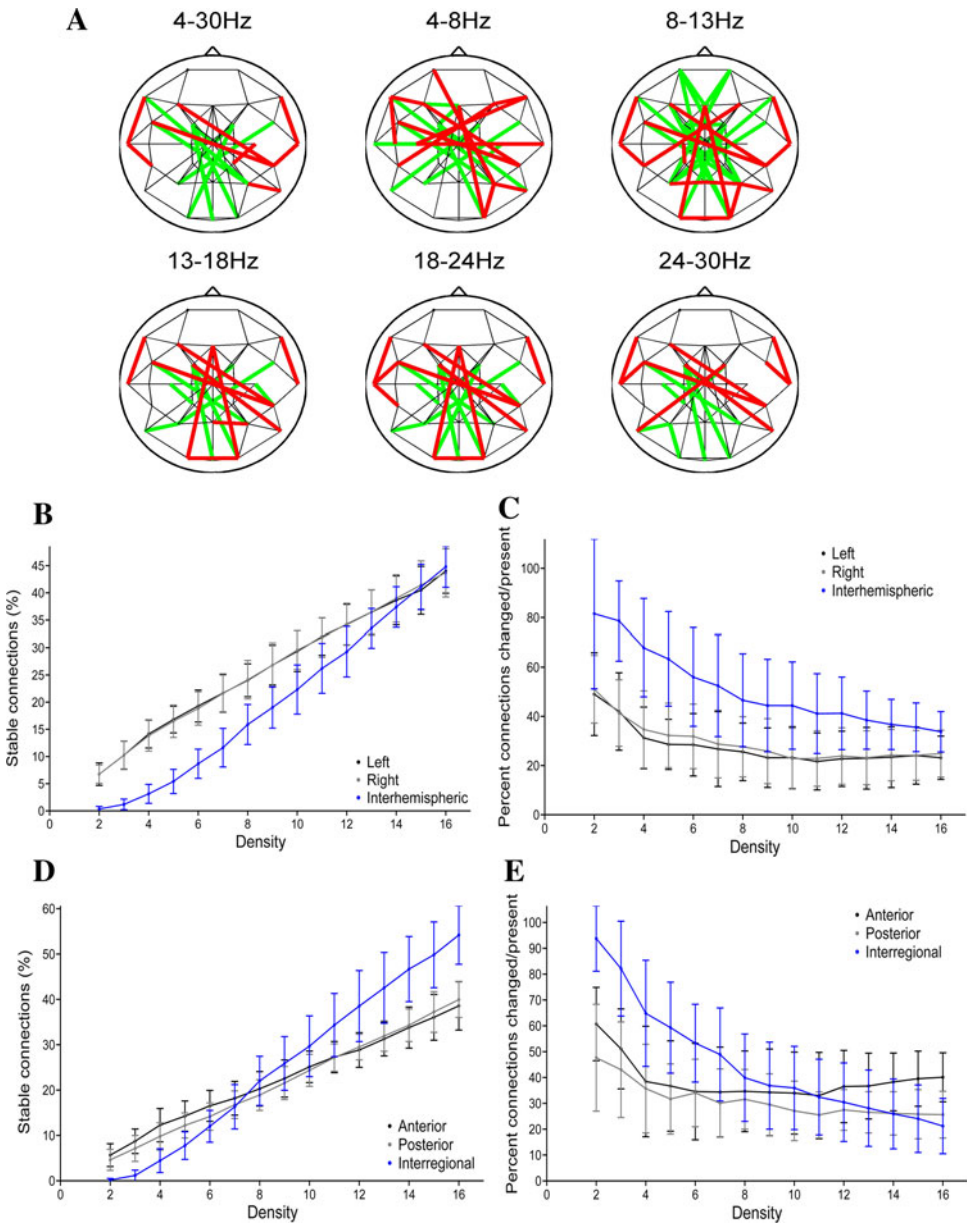

Fig. 6 Network topologies and cTBSin fixed-density networks. **a** Fixed-density networks for the average (across-subject) lagged max covariance data in different frequency bands. These graphs are constructed by applying a threshold to produce networks with a mean nodal connectivity degree of four (an average of four connections per node), with thresholds set independently in both the pre-cTBS and post-cTBS periods. Connections present both pre- and post-cTBS are depicted in *black*, connections present only prior to cTBS in *green*, and connections present only after cTBS are shown in *red*. **b** The percentage of broad-band connections that are present and stable (present both before and after rTMS) as a function of hemisphere and density. **c** The broad-band modulation index (percent of connections modified/percentage of connections present in either or both periods) as a function of hemisphere and density. **d** The percentage of broad-band connections that are present and stable as a function of region and density. **e** The broad-band modulation index as a function of region and density

anterior to posterior regions also varied as a function of connection density (broad band in Fig. 6d and e; other frequency bands in Supplementary Figs. 3–4). For the percent of stable connections (unchanged by cTBS), along the anterior–posterior axis, there is a main effect of connection region ($F(2,24) = 5.1$; $p = 0.01$), with significantly more unchanged connections present interregionally than posteriorly (Fig. 6d; marginal means 25.7 versus 22.0, $p < 0.05$). Additionally, there is a significant interaction ($F(28,336) = 46.1$, $p < 0.001$), with fewer interregional than anterior or posterior unchanged connections when thresholds are applied to produce networks with low connection densities, but greater interregional than anterior or posterior connections at high connection densities (Fig. 6d). These findings are consistent with the presence of numerous connections of moderate strength *between* regions, versus distinct smaller sets of strong and very weak connections *within* each region. At low connection densities, the interregional connections between anterior and posterior regions are the ones whose presence is most likely to be modulated by cTBS, while at high connection densities the connections within the anterior region are most likely to be modulated (Fig. 6e). Again, similar patterns are present in other frequency bands (Supplementary Figs. 3–4).

For the variable-density networks, the threshold was set to produce graphs with a specific mean connectivity degree before cTBS, and this same threshold was then applied to

the MC values after cTBS. To illustrate, Fig. 7a shows the networks that result when the threshold is set to produce a connection density of four connections per node in the pre-cTBS period. There are clear frequency-specific differences in the induced network changes. Specifically, there are fewer edges (connections) in the post-cTBS network than in the pre-cTBS network in the alpha frequency band (strengthening index <1), while there are more edges in the post-cTBS than pre-cTBS network in the beta frequency bands (strengthening index >1). The decrease in the number of alpha-band connections after cTBS is seen across network densities, although with shifting regional and hemispheric prevalence (Fig. 7b and c). In comparison, the increase in the number of connections after cTBS in the high-beta band also occurs regardless of connection density, but with the greatest effects consistently seen in anterior and interhemispheric connections (Fig. 7d and e).

cTBS Produces Changes in Graph Theory Statistics

Graph topological indices were systematically calculated for the fixed-density networks across densities. For the clustering coefficient, there is a significant main effect of pre- versus post-cTBS period, with an increase in clustering after cTBS in the broad- (Fig. 8a; $F(1,12) = 5.3$, $p = 0.04$), theta- (Fig. 8b; $F(1,12) = 28.9$; $p < 0.001$) and low-beta- (Fig. 8c; $F(1,12) = 7.3$; $p = 0.02$) bands. There is no significant effect of period on the path length in any frequency band (not shown). The increase in the clustering coefficient after cTBS is not simply due to an increase in connectivity between geographically close electrodes, as there is no relationship between inter-electrode geodesic distance and the change in connectivity strength after cTBS (Supplementary Fig. 5). Finally, in the variable-density networks, we assessed changes in node degree after cTBS for each frequency band, to determine which electrodes show the greatest changes in connectivity (Fig. 8d). In the theta band, there was a significant decrease in node degree ($F(1,12) > 16.4$, Bonferroni corrected $p < 0.05$) for the C1 and Cz electrodes, as well as a significant increase for the F8 electrode. In the alpha band, there were significant decreases in node degree in a region immediately anteromedial to the site of stimulation (the FC1, FC2, Fz, C1 and Cz electrodes), as well as in posterior regions (P3, Pz, P4, O1, Oz). In the high beta band, there were significant increases in connectivity in the left frontocentral region (Fp1, F7, FC5), as well as in the F8 and CP2 electrodes. There were no significant changes in node degree in the broad, low-beta or mid-beta bands. Consequently, the global mean connectivity degree is decreased in the alpha frequency band ($F(1,14) = 16.6$, $p = 0.0015$), while the global mean connectivity degree is increased in the high-beta frequency bands ($F(1,14) = 12.01$, $p = 0.005$).

Discussion

Network Connectivity Changes After cTBS

In the present study, we applied network analysis techniques to understand the changes that occur in EEG functional connectivity networks after cTBS is applied to primary motor cortex. The continuous theta-burst technique that was applied has previously been shown to produce a significant decrease in cortico-spinal excitability, as measured via motor-evoked potentials (Huang et al. 2005). Di Lazzaro et al. (2005) have shown that this decrease in MEP size is due to a decrease in the excitability of local cortical circuits generating the I1 wave of corticospinal output. Therefore, EEG seems well suited to further characterize the neurobiological substrate of the lasting modulatory effects of cTBS of brain excitability.

We found that after cTBS was applied to the primary motor cortex, there was a frequency-specific change in the pattern of connectivity, with significant decreases in functional connectivity in the alpha band, and significant increases in functional connectivity in the beta and broad bands. There was also a regional specificity in the pattern of EEG functional connectivity changes, with significant changes noted most commonly in the anterior/interregional and interhemispheric connections. When EEG network topologies were examined before and after cTBS, intrahemispheric connections were commonly present both before and after cTBS, whereas interhemispheric connections were less prevalent, especially at lower connection densities, but were more likely to have been altered. The subsequent graph theoretical analysis revealed that there was a significant increase in the clustering coefficient, and thus efficiency of local information processing, in the broadband, theta and low-beta frequencies. The nodal connectivity degree of a subset of nodes anteromedial to the stimulation site was decreased after cTBS, particularly in the theta and alpha bands, suggesting that the connectivity of these electrodes with the rest of the brain was decreased. In contrast, there was an increase in nodal degree (connectivity) in the left frontocentral, right frontal and right centroparietal region after cTBS in the high beta band. Thus, the results suggest that cTBS results in a patterned modulation of EEG functional connectivity and network topology in the human brain. Since cTBS was applied at an intensity low enough to avoid induction of motor twitching, the changes in EEG networks are unlikely to be caused by afferent input following cortico-spinal effects of TMS, and instead presumably reflect the direct cortical network impact of TMS.

Previous studies utilizing a variety of neuroimaging techniques have demonstrated that rTMS applied to a single area modulates the activity of widespread cortical networks (Bestmann et al. 2003, 2005; Chouinard et al.

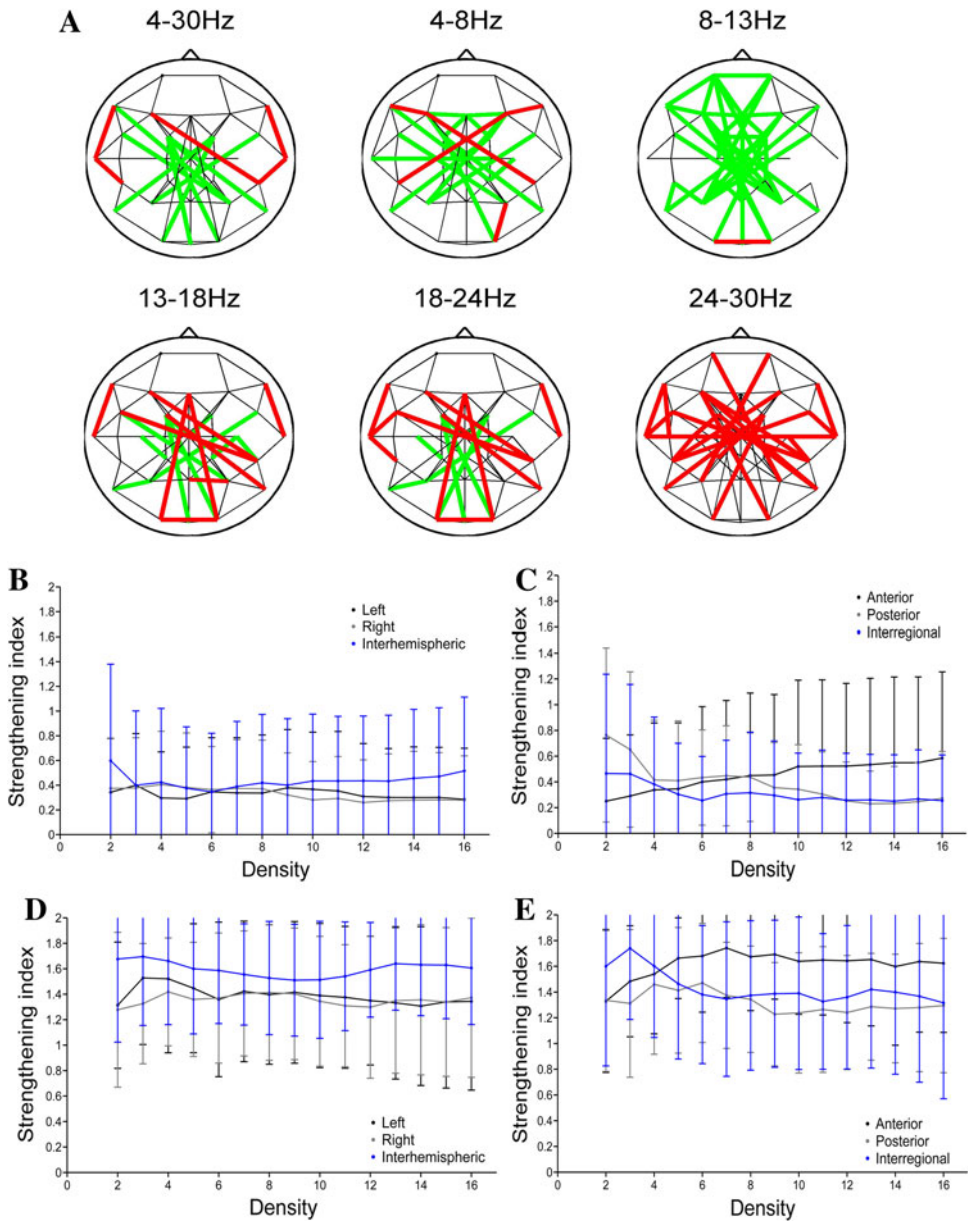

Fig. 7 Network topologies and cTBS in variable density networks. **a** Variable-density networks in different frequency bands. The thresholds used to construct these graphs are selected to produce networks with a mean nodal degree of four in the pre-cTBS period; the same threshold is then applied to the data from the post-cTBS period. Connections present both pre- and post-cTBS are depicted in *black*, connections present only prior to cTBS in *green*, and connections present only after cTBS are shown in *red*. **b** The strengthening index (percentage of connections strengthened × 2/percentage of connections changed) in the alpha band as a function of hemisphere and density. **c** The strengthening index in the alpha band as a function of region and density. **d** The strengthening index in the high-beta band as a function of hemisphere and density. **e** The strengthening index in the high-beta band as a function of region and density

2003; Jing and Takigawa 2000; Plewnia et al. 2008). Furthermore, a number of studies combining rTMS with EEG have shown that rTMS to a given cortical region alters the functional connectivity of that region with other cortical areas (Chen et al. 2003; Fuggetta et al. 2008; Jing and Takigawa 2000; Oliviero et al. 2003; Plewnia et al. 2008; Strens et al. 2002), with the precise pattern of changes varying as a function of particular rTMS protocol applied and frequency band analyzed. However, one consistent finding across all studies was that the biggest changes were seen in the alpha band, such that high-frequency rTMS generally produces decreases in alpha-band coherence, while low-frequency rTMS generally is to found result in increased coherence in the alpha band (although an increase in alpha-band coherence was noted after high-frequency rTMS in Jing and Takigawa (2000). Notably, however, none of the previous studies evaluating EEG functional connectivity changes after rTMS utilized a theta-burst stimulation protocol, as in this study. Similarly, Polania et al. (2011a) applied anodal (facilitatory) tDCS to the left motor region, and utilized functional connectivity network analysis techniques to demonstrate that in resting state networks tDCS produced increased synchronization within the frontal regions in the theta, alpha and beta bands. During task performance, there was a frequency band-dependent increase in synchronization within the ipsilateral hemisphere, as well as significant interhemispheric desynchronization in the α, β and high-γ bands.

Our study represents the first analysis of network-level connectivity changes after cTBS rTMS. Some of the results

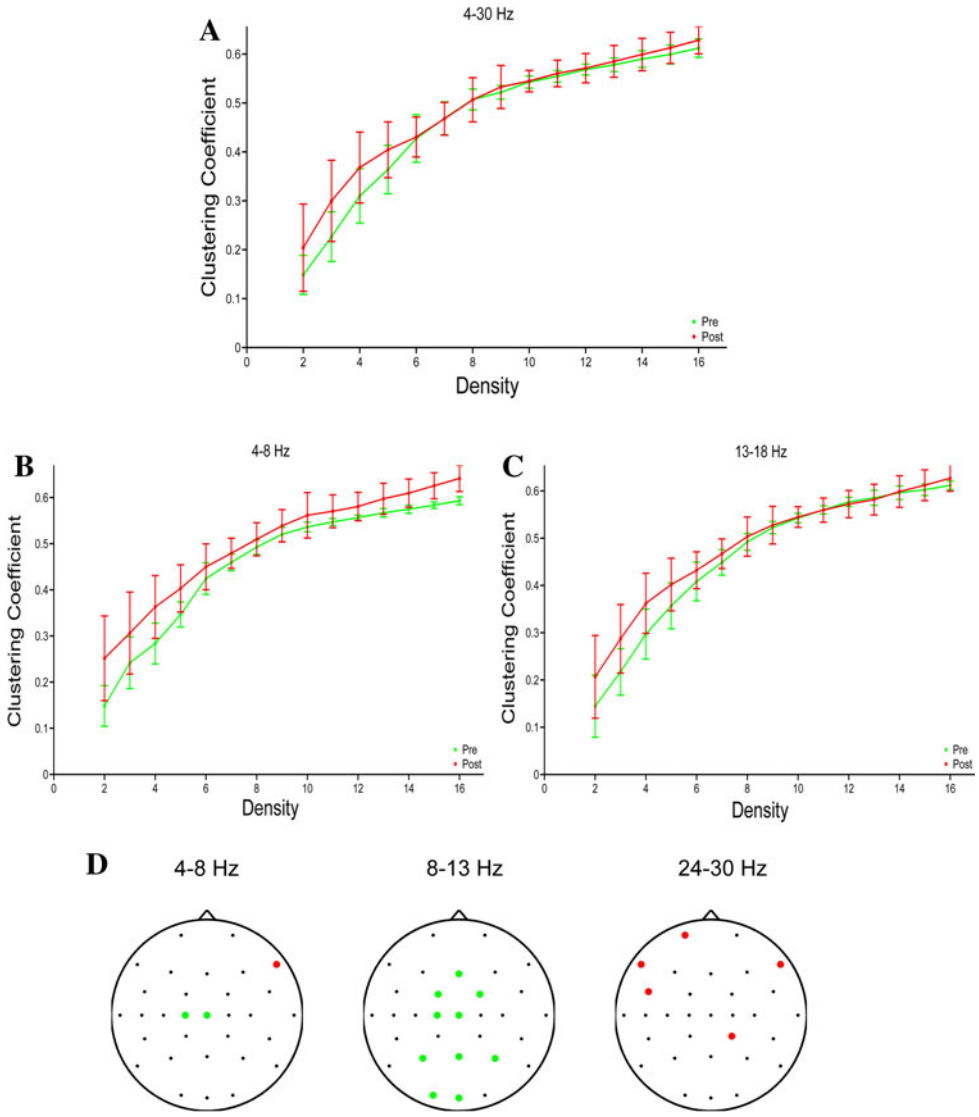

Fig. 8 Graph theory metrics. **a** Clustering coefficient pre- and post-cTBS as a function of density in the broad band in the fixed-density networks. **b** Clustering coefficient in the theta band in the fixed-density networks. **c** Clustering coefficient in the in the low-beta band in the fixed-density networks. **d** Channels with significant changes in node degree after cTBS in the variable-density networks. The *green dots* indicate electrodes with a significant decrease in node degree after rTMS, while the *red dots* indicate electrodes with a significant increase in node degree. No significant changes were seen in other frequency bands

are consistent with and extend previous research, such as the finding that the largest changes are in the alpha band.In contrast, the dissociation between the functional connectivity changes in the different frequency bands (decreased after cTBS in the alpha band, increased in beta) is a novel finding, and suggests that the cTBS protocol used in this study has differential effects on the functional architectures that underlie these different frequencies. This study is also the first to assess changes in network topologies after cTBS, and the resulting effects on graph theoretic measures of information processing efficiency.

Regional and Band-specific Changes in Functional Connectivity

Our study demonstrates clear frequency band- and region-specific effects of cTBS on functional connectivity. Across subjects, the most frequent changes occur in the alpha band (Figs. 4, 5, 6, 8), in which a substantial majority of connections show decreased functional connectivity after cTBS in all regions (Figs. 3, 4, 5, 7). These findings are consistent with previous work demonstrating that rTMS modulates alpha-band functional connectivity (Brignani et al. 2008; Hamidi et al. 2009; Jing and Takigawa 2000; Oliviero et al. 2003; Schindler et al. 2008; Strens et al. 2002). However, the direction of the change (a significant decrease in alpha-band connectivity following exposure to an cTBS protocol known to generally suppress cortical excitability) conflicts with some of the previous results. This difference may be due to the different stimulation protocol (cTBS instead of fixed-frequency rTMS) used in this study. Another explanation is that the analysis techniques were different in the other studies. For example, Strens et al. (2002) used a simple coherence analysis with bipolar derivations, thus potentially underestimating the TMS induced changes. Brignani et al. (2008) and Hamidi

et al. (2009) did not test for connectivity changes after rTMS, but over frequency power; moreover Hamidi et al. (2009) tested the effects during a working memory task. A large number of connections are also altered in the high-beta (24–30 Hz) band. However, in contrast to the decrease in alpha-band connectivity, functional connectivity within the beta band is increased after cTBS (Figs. 4, 5,7), most prominently in the anterior regions (Fig. 4). Furthermore, functional connectivity in the theta band tends to increase in frontal regions after cTBS, but decreases in posterior regions and between regions (Fig. 4). Consequently, we demonstrate a dissociation between the effects of cTBS in the different frequency bands and across regions.

Increases in alpha activity have traditionally been associated with predominantly inhibitory activities, with decreases in alpha coherence seen in a variety of cognitive tasks (Klimesch et al. 2007; Neuper and Pfurtscheller 2001; Pfurtscheller 2003), although recent studies have disputed this interpretation (Palva and Palva 2007). Notably, recent studies have reported a decrease in alpha-band functional connectivity in the ipsilesional central electrodes in patients with stroke, and alpha-band connectivity was correlated with motor task performance (Dubovik et al. 2012). Increases in high-frequency activities, typically gamma-band, have also been associated with active information processing, and perhaps binding of information across regions (Buzsáki and Draguhn 2004; Fries et al. 2007; Gregoriou et al. 2009; Jutras et al. 2009). Furthermore, increases in beta and gamma-band functional connectivity either in preparation for or during motor tasks have been reported within the sensorimotor network, frontal eye fields, and prefrontal cortices (Wheaton et al. 2005; Bardouille and Boe 2012; Herz et al. 2012). In this study, a global decrease in functional connectivity was seen in the alpha band, along with a frontally-predominant increase in functional connectivity within the high-beta band. There were also complex spatially segregated changes in theta band functional connectivity after cTBS. These changes in functional connectivity values resulted in a decrease in alpha-band (and to a lesser degree theta-band) nodal degree anteromedial to the site of stimulation (Fig. 8d), and an increase in nodal degree in the beta bands in the left frontocentral, right centroparietal and right frontal regions. Taken together, these results suggest the hypothesis that there is a decrease in inhibitory global functional connectivity, and a functional disconnection of the region anteriomedial to the site of stimulation. The decreases in alpha-band connectivity in the electrodes anteromedial to the site of stimulation may be related to the decreased excitability of motor cortex typically produced by cTBS to this region. The increase in the clustering coefficient noted in the graph theoretic analysis, discussed further below, is also consistent with this hypothesis.

At first glance, the complex spatially segregated changes in theta-band functional connectivity (especially the decrease in nodal degree at the site of stimulation) seen in the present study may appear to conflict with recent studies in which short bursts of rTMS entrain cortical oscillations in the relevant frequency band (Hamidi et al. 2009; Thut et al. 2011), with implications for cognitive performance (Klimesch et al. 2003; Hamidi et al. 2009; Thut et al. 2011; Romei et al. 2011). However, in those prior studies, rTMS was applied as short trains (5–30 pulses) in frequencies that typically cause increases of cortical excitability. In contrast, in the current study, a different stimulation protocol (inhibitory continuous theta-burst stimulation) with a more complex stimulation pattern (3 pulses at 50 Hz repeated at 5 Hz, versus a fixed frequency stimulation in the prior studies) was applied for a longer period of time, and at significantly lower intensity (80 % AMT in the current study, vs 100 % phosphene threshold in the study of Thut et al. 2011, and 110 % RMT in the study of Hamidi et al. 2009). Thus, the different results could be attributed to different stimulation paradigms. More importantly, changes in connectivity were assessed over longer periods of time in the current study (10 min following at least 30 s after the end of cTBS stimulation, versus in the seconds immediately after stimulation in the prior studies). While the behavioral effects of short trains of TMS pulses may be accomplished through entrainment of ongoing cortical oscillations, the long-lasting effects of longer TMS trains are probably accomplished via a different mechanism (induction of synaptic plasticity), with less predictable shifts in cortical rhythms.

Hemispheric Changes in Functional Connectivity

Even though cTBS was applied to the left motor cortex in our study, significantly more interhemispheric connections were modulated than within the left (or right) hemisphere. Furthermore, while the absolute change in functional connectivity strength varies as a function of frequency, the interhemispheric connections were more likely to be strengthened after cTBS than the intrahemispheric connections across all frequency bands (Fig. 5d). Taken together, these findings suggest that the continuous theta-burst protocol used in this study may increase functional coupling between the two hemispheres, and possibly decrease MEP size, by increasing the interhemispheric inhibition to the target region, as may occur after stroke (Grefkes and Fink 2011; Murase et al. 2004). Alternatively, the relative strengthening of interhemispheric functional connectivity may be a result of recruitment of contralateral brain regions to dynamically compensate for locally suppressed cortical activity, as other work has suggested may also occur after stroke (Carter et al. 2010; Gerloff et al. 2006;

Lotze et al. 2006) and after inhibitory rTMS (O'Shea et al. 2007). Increased coupling between the hemispheres and recruitment of contralateral brain regions may also explain why focal left motor stimulation did not produce greater changes in the left than right hemisphere.

Modulation of Network Topology

We explored the changes in network topology that occur after cTBS by examining the undirected graphs that result from applying a threshold to the maximum-correlation values for all electrode pairs. In one set of analyses, the thresholds for each time period (before and after cTBS) were set independently to produce networks with an identical number of connections in each period (fixed-density networks). In the resulting graphs, intrahemispheric and intraregional connections that are present both before and after cTBS are significantly more common than interhemispheric or interregional connections when the thresholds are set to produce networks with low connection densities. In contrast, when thresholds are set low to produce networks with high connection densities, the number of stable interhemispheric connections is equal to the number of intrahemispheric connections, while the number of interregional connections is greater than the number of intraregional connections. Thus, these graphs show that the majority of strong functional connections are short-range or local, consistent with anatomical data demonstrating greater *structural* connectivity between adjacent rather than distant cortical regions (Hagmann et al. 2008; Kaiser and Hilgetag 2004; Lewis et al. 2009), and with prior EEG and fMRI studies demonstrating greater *functional* connectivity between adjacent cortical regions (Honey et al. 2009; Salvador et al. 2005; Srinivasan et al. 2007). However, these studies also show that the connections between hemispheres and regions are of moderate strength, while there are areas within hemispheres and regions that are only weakly connected. The presence of moderately strong interhemispheric functional connectivity is consistent with the presence of significant transcallosal anatomic connectivity between homologous areas, while the moderately strong interregional functional connectivity is consistent with the presence of functionally integrated, spatially distributed networks within regions. More importantly, the presence of areas within hemispheres and regions that have a relative lack of functional connectivity is consistent with the idea that the human brain is organized into anticorrelated functional networks (Fox et al. 2005, 2009).

While the interhemispheric connections are significantly less common, especially at low connection densities, their presence was significantly more likely to be modulated by cTBS (i.e. present only before or after cTBS, but not in both periods). The interregional connections are also less prevalent and more likely to be modulated by cTBS at low connection densities, while the anterior connections are less prevalent and more likely to be modulated by cTBS at high connection densities. Furthermore, these graphs also demonstrated that global connectivity is decreased in the alpha bands, and increased in the beta bands. Previous work has suggested that TMS has state-dependent effects, with a number of studies demonstrating that single-pulse TMS preferentially affects the least active neuronal populations (see Silvanto and Pascual-Leone (2008), for review). Furthermore, fMRI work has suggested that TMS can either strengthen or weaken functional connectivity depending on the initial activity states of the relevant regions (Bestmann et al. 2008). Similar findings regarding state-dependency and preferential modulation of the (presumptive) least active neuronal populations have also been demonstrated for theta-burst rTMS protocols (Silvanto et al. 2008). This preferential modulation of less active populations may provide an explanation for our finding that cTBS is more likely to affect the strength of interregional and interhemispheric connections rather than intraregional or intrahemispheric connections, even though the latter are more likely to be present.

Network Topological Changes

The graph theoretical analyses reveal that in the fixed-density networks, there is a significant increase in the clustering coefficient after cTBS in the theta and low-beta bands, as well as in the broad band. The clustering coefficient quantifies the degree to which the nearest neighbors of a given node are connected to each other, and thereby represents a measure of the degree of local connectivity (Bullmore and Sporns 2009; Reijneveld et al. 2007; Watts and Strogatz 1998). High clustering has traditionally been interpreted as supporting a high efficiency of local information processing, and robustness to random error or network damage (Bullmore and Sporns 2009; Latora and Marchiori 2003). In contrast, the mean path length, which is the average of the minimum number of edges that must be traversed to go from any one node to any other node, and is inversely related to the efficiency of global information transfer (Bullmore and Sporns 2009; Latora and Marchiori 2003), did not change. Networks with relatively high clustering coefficients and relatively short mean path lengths are known as small world networks (Bullmore and Sporns 2009; Reijneveld et al. 2007; Watts and Strogatz 1998). Such small-world networks possess high complexity, defined as a near optimal balance between local specialization and global integration (Sporns et al. 2000). In the present study, after cTBS there is an increase in the local efficiency of information processing in the theta, low-beta and broad bands, as indicated by the increase in the clustering coefficient. The lack of significant

changes in path length within these bands indicates that there is no significant change of global efficiency. The increase in local efficiency without loss of global efficiency suggests that the network adopts a more "small-world" topology (Fig. 8b). Notably, a recent study reported an increase in small-world properties and functional integration in the beta band during motor task performance (Jin et al. 2012). The increase in clustering noted in the current study is consistent with this finding, and suggests that the motor network may be dynamically reorganizing to minimize the disruptive effects of the local "virtual lesion" produced by cTBS. Importantly, the increase in clustering after cTBS was not simply due to an increase in connectivity between anatomically close regions, highlighting that "clustering" in the graph-theoretic sense does not necessarily imply anatomic proximity.

Conclusions

In summary, in the present study functional connectivity and network analysis techniques reveal that after cTBS to motor cortex, there are significant widespread changes in cortical functional connectivity, with the specific changes occurring in a region, hemisphere and frequency-specific manner. These changes lead to shifts in the cortical functional network topology, with implications for network complexity and efficiency of information processing. Thus, network analysis techniques provide a highly promising tool for evaluating the effects of brain stimulation paradigms on cortical function. Future studies should combine such network analysis techniques with protocols directly assessing cortical excitability, protocols targeting different brain regions, and with various behavioral paradigms, to assess how TMS-induced network changes are related to changes in local cortical excitability, cortical target region, and behavioral task performance.

Acknowledgments Work on this study was supported by grants from the National Center for Research Resources: Harvard Clinical and Translational Science Center (UL1 RR025758), Center for Integration of Medicine and Innovative Technology (CIMIT), the Sidney R. Baer, Jr. Foundation, and Nexstim to APL. MMS was supported by funds from the National Center for Research Resources: Harvard Clinical and Translational Science Center (UL1 RR025758), and the Center for Integration of Medicine and Innovative Technology (CIMIT). MBW and SSC receive research support from the NIH/NINDS (RO1-NS062092). LO was supported by NIH fellowship F32MH080493 and 1KL2RR025757-01.

Disclosures MMS, MBW, LO and SSC report no conflicts of interest. APL serves on the scientific advisory boards for Nexstim, Neuronix, Starlab Neuroscience, Allied Mind, Neosync, and Novavision, and is an inventor on patents and patent applications related to noninvasive brain stimulation and the real-time integration of transcranial magnetic stimulation with electroencephalography and magnetic resonance imaging.

References

Achard S, Bullmore E (2007) Efficiency and cost of economical brain functional networks. PLoS Comput Biol 3:e17

Bardouille T, Boe S (2012) State-related changes in MEG functional connectivity reveal the task-positive sensorimotor network. PLoS One 7:e48682

Barker AT, Jalinous R, Freeston IL (1985) Non-invasive magnetic stimulation of human motor cortex. Lancet 1:1106–1107

Bestmann S, Baudewig J, Siebner HR, Rothwell JC, Frahm J (2003) Subthreshold high-frequency TMS of human primary motor cortex modulates interconnected frontal motor areas as detected by interleaved fMRI-TMS. Neuroimage 20:1685–1696

Bestmann S, Baudewig J, Siebner HR, Rothwell JC, Frahm J (2004) Functional MRI of the immediate impact of transcranial magnetic stimulation on cortical and subcortical motor circuits. Eur J Neurosci 19:1950–1962

Bestmann S, Baudewig J, Siebner HR, Rothwell JC, Frahm J (2005) BOLD MRI responses to repetitive TMS over human dorsal premotor cortex. Neuroimage 28:22–29

Bestmann S, Ruff CC, Blankenburg F, Weiskopf N, Driver J, Rothwell JC (2008) Mapping causal interregional influences with concurrent TMS-fMRI. Exp Brain Res 191:383–402

Brignani D, Manganotti P, Rossini PM, Miniussi C (2008) Modulation of cortical oscillatory activity during transcranial magnetic stimulation. Hum Brain Mapp 29:603–612

Bullmore E, Sporns O (2009) Complex brain networks: graph theoretical analysis of structural and functional systems. Nat Rev Neurosci 10:186–198

Buzsáki G, Draguhn A (2004) Neuronal oscillations in cortical networks. Science 304:1926–1929

Carter AR, Astafiev SV, Lang CE, Connor LT, Rengachary J, Strube MJ, Pope DLW, Shulman GL, Corbetta M (2010) Resting interhemispheric functional magnetic resonance imaging connectivity predicts performance after stroke. Ann Neurol 67:365–375

Chen R, Classen J, Gerloff C, Celnik P, Wassermann EM, Hallett M, Cohen LG (1997) Depression of motor cortex excitability by low-frequency transcranial magnetic stimulation. Neurology 48:1398–1403

Chen W-H, Mima T, Siebner HR, Oga T, Hara H, Satow T, Begum T, Nagamine T, Shibasaki H (2003) Low-frequency rTMS over lateral premotor cortex induces lasting changes in regional activation and functional coupling of cortical motor areas. Clin Neurophysiol 114:1628–1637

Chouinard PA, Van Der Werf YD, Leonard G, Paus T (2003) Modulating neural networks with transcranial magnetic stimulation applied over the dorsal premotor and primary motor cortices. J Neurophysiol 90:1071–1083

Delorme A, Makeig S (2004) EEGLAB: an open source toolbox for analysis of single-trial EEG dynamics including independent component analysis. J Neurosci Methods 134:9–21

Di Lazzaro V, Pilato F, Saturno E, Oliviero A, Dileone M, Mazzone P, Insola A, Tonali PA, Ranieri F, Huang YZ, Rothwell JC (2005) Theta-burst repetitive transcranial magnetic stimulation suppresses specific excitatory circuits in the human motor cortex. J Physiol 565:945–950

Dubovik S, Pignat J-M, Ptak R, Aboulafia T, Allet L, Gillabert N, Magnin C, Albert F, Momjian-Mayor I, Nahum L, Lascano AM, Michel CM, Schnider A, Guggisberg AG (2012) The behavioral significance of coherent resting-state oscillations after stroke. Neuroimage 61:249–257

Esser SK, Huber R, Massimini M, Peterson MJ, Ferrarelli F, Tononi G (2006) A direct demonstration of cortical LTP in humans: a combined TMS/EEG study. Brain Res Bull 69:86–94

Fox MD, Snyder AZ, Vincent JL, Corbetta M, Van Essen DC, Raichle ME (2005) The human brain is intrinsically organized into dynamic, anticorrelated functional networks. Proc Natl Acad Sci USA 102:9673–9678

Fox MD, Zhang D, Snyder AZ, Raichle ME (2009) The global signal and observed anticorrelated resting state brain networks. J Neurophysiol 101:3270–3283

Fox MD, Buckner RL, White MP, Greicius MD, Pascual-Leone A (2012) Efficacy of transcranial magnetic stimulation targets for depression is related to intrinsic functional connectivity with the subgenual cingulate. Biol Psychiatry 72:595–603

Fries P, Nikolić D, Singer W (2007) The gamma cycle. Trends Neurosci 30:309–316

Fuggetta G, Pavone EF, Fiaschi A, Manganotti P (2008) Acute modulation of cortical oscillatory activities during short trains of high-frequency repetitive transcranial magnetic stimulation of the human motor cortex: a combined EEG and TMS study. Hum Brain Mapp 29:1–13

Garcia JO, Grossman ED, Srinivasan R (2011) Evoked potentials in large-scale cortical networks elicited by TMS of the visual cortex. J Neurophysiol 106:1734–1746

Gerloff C, Bushara K, Sailer A, Wassermann EM, Chen R, Matsuoka T, Waldvogel D, Wittenberg GF, Ishii K, Cohen LG, Hallett M (2006) Multimodal imaging of brain reorganization in motor areas of the contralesional hemisphere of well recovered patients after capsular stroke. Brain 129:791–808

Grefkes C, Fink GR (2011) Reorganization of cerebral networks after stroke: new insights from neuroimaging with connectivity approaches. Brain 134:1264–1276

Grefkes C, Nowak DA, Wang LE, Dafotakis M, Eickhoff SB, Fink GR (2010) Modulating cortical connectivity in stroke patients by rTMS assessed with fMRI and dynamic causal modeling. Neuroimage 50:233–242

Gregoriou GG, Gotts SJ, Zhou H, Desimone R (2009) High-frequency, long-range coupling between prefrontal and visual cortex during attention. Science 324:1207–1210

Hagmann P, Cammoun L, Gigandet X, Meuli R, Honey CJ, Wedeen VJ, Sporns O (2008) Mapping the structural core of human cerebral cortex. PLoS Biol 6:e159

Hamidi M, Slagter HA, Tononi G, Postle BR (2009) Repetitive transcranial magnetic stimulation affects behavior by biasing endogenous cortical oscillations. Front Integr Neurosci 3:14

He Y, Dagher A, Chen Z, Charil A, Zijdenbos A, Worsley K, Evans A (2009) Impaired small-world efficiency in structural cortical networks in multiple sclerosis associated with white matter lesion load. Brain 132:3366–3379

Herz DM, Christensen MS, Reck C, Florin E, Barbe MT, Stahlhut C, Pauls KAM, Tittgemeyer M, Siebner HR, Timmermann L (2012) Task-specific modulation of effective connectivity during two simple unimanual motor tasks: a 122-channel EEG study. Neuroimage 59:3187–3193

Hilgetag CC, Théoret H, Pascual-Leone A (2001) Enhanced visual spatial attention ipsilateral to rTMS-induced "virtual lesions" of human parietal cortex. Nat Neurosci 4:953–957

Honey CJ, Sporns O, Cammoun L, Gigandet X, Thiran JP, Meuli R, Hagmann P (2009) Predicting human resting-state functional connectivity from structural connectivity. PNAS 106:2035–2040

Huang Y-Z, Edwards MJ, Rounis E, Bhatia KP, Rothwell JC (2005) Theta burst stimulation of the human motor cortex. Neuron 45:201–206

Huang Y-Z, Chen R-S, Rothwell JC, Wen H-Y (2007) The after-effect of human theta burst stimulation is NMDA receptor dependent. Clin Neurophysiol 118:1028–1032

Ilmoniemi RJ, Virtanen J, Ruohonen J, Karhu J, Aronen HJ, Näätänen R, Katila T (1997) Neuronal responses to magnetic stimulation reveal cortical reactivity and connectivity. Neuroreport 8:3537–3540

Jin S-H, Lin P, Hallett M (2012) Reorganization of brain functional small-world networks during finger movements. Hum Brain Mapp 33:861–872

Jing H, Takigawa M (2000) Observation of EEG coherence after repetitive transcranial magnetic stimulation. Clin Neurophysiol 111:1620–1631

Jutras MJ, Fries P, Buffalo EA (2009) Gamma-band synchronization in the macaque hippocampus and memory formation. J Neurosci 29:12521–12531

Kaiser M, Hilgetag CC (2004) Modelling the development of cortical systems networks. Neurocomputing 58–60:297–302

Khedr EM, Abdel-Fadeil MR, Farghali A, Qaid M (2009) Role of 1 and 3 Hz repetitive transcranial magnetic stimulation on motor function recovery after acute ischaemic stroke. Eur J Neurol 16:1323–1330

Klimesch W, Sauseng P, Gerloff C (2003) Enhancing cognitive performance with repetitive transcranial magnetic stimulation at human individual alpha frequency. Eur J Neurosci 17:1129–1133

Klimesch W, Sauseng P, Hanslmayr S (2007) EEG alpha oscillations: the inhibition-timing hypothesis. Brain Res Rev 53:63–88

Komssi S, Aronen HJ, Huttunen J, Kesäniemi M, Soinne L, Nikouline VV, Ollikainen M, Roine RO, Karhu J, Savolainen S, Ilmoniemi RJ (2002) Ipsi- and contralateral EEG reactions to transcranial magnetic stimulation. Clin Neurophysiol 113:175–184

Latora V, Marchiori M (2003) Economic small-world behavior in weighted networks. Eur Phys J B 32:249–263

Lewis JD, Theilmann RJ, Sereno MI, Townsend J (2009) The relation between connection length and degree of connectivity in young adults: a DTI analysis. Cereb Cortex 19:554–562

Lotze M, Markert J, Sauseng P, Hoppe J, Plewnia C, Gerloff C (2006) The role of multiple contralesional motor areas for complex hand movements after internal capsular lesion. J Neurosci 26:6096–6102

Maeda F, Keenan JP, Tormos JM, Topka H, Pascual-Leone A (2000) Modulation of corticospinal excitability by repetitive transcranial magnetic stimulation. Clin Neurophysiol 111:800–805

May A, Hajak G, Gänssbauer S, Steffens T, Langguth B, Kleinjung T, Eichhammer P (2007) Structural brain alterations following 5 days of intervention: dynamic aspects of neuroplasticity. Cereb Cortex 17:205–210

Murase N, Duque J, Mazzocchio R, Cohen LG (2004) Influence of interhemispheric interactions on motor function in chronic stroke. Ann Neurol 55:400–409

Neuper C, Pfurtscheller G (2001) Event-related dynamics of cortical rhythms: frequency-specific features and functional correlates. Int J Psychophysiol 43:41–58

Newman MEJ (2003) The structure and function of complex networks. SIAM Review 45:167–256

O'Shea J, Johansen-Berg H, Trief D, Göbel S, Rushworth MFS (2007) Functionally specific reorganization in human premotor cortex. Neuron 54:479–490

Oliviero A, Strens LHA, Di Lazzaro V, Tonali PA, Brown P (2003) Persistent effects of high frequency repetitive TMS on the coupling between motor areas in the human. Exp Brain Res 149:107–113

Palva S, Palva JM (2007) New vistas for α-frequency band oscillations. Trends Neurosci 30:150–158

Pascual-Leone A, Valls-Solé J, Wassermann EM, Hallett M (1994) Responses to rapid-rate transcranial magnetic stimulation of the human motor cortex. Brain 117(Pt 4):847–858

Paus T, Jech R, Thompson CJ, Comeau R, Peters T, Evans AC (1997) Transcranial magnetic stimulation during positron emission tomography: a new method for studying connectivity of the human cerebral cortex. J Neurosci 17:3178–3184

Pfurtscheller G (2003) Induced oscillations in the alpha band: functional meaning. Epilepsia 44(Suppl 12):2–8

Plewnia C, Rilk AJ, Soekadar SR, Arfeller C, Huber HS, Sauseng P, Hummel F, Gerloff C (2008) Enhancement of long-range EEG coherence by synchronous bifocal transcranial magnetic stimulation. Eur J Neurosci 27:1577–1583

Polanía R, Nitsche MA, Paulus W (2011a) Modulating functional connectivity patterns and topological functional organization of the human brain with transcranial direct current stimulation. Hum Brain Mapp 32:1236–1249

Polanía R, Paulus W, Antal A, Nitsche MA (2011b) Introducing graph theory to track for neuroplastic alterations in the resting human brain: a transcranial direct current stimulation study. Neuroimage 54:2287–2296

Reijneveld JC, Ponten SC, Berendse HW, Stam CJ (2007) The application of graph theoretical analysis to complex networks in the brain. Clin Neurophysiol 118:2317–2331

Romei V, Driver J, Schyns PG, Thut G (2011) Rhythmic TMS over parietal cortex links distinct brain frequencies to global versus local visual processing. Curr Biol 21:334–337

Rubinov M, Knock SA, Stam CJ, Micheloyannis S, Harris AWF, Williams LM, Breakspear M (2009) Small-world properties of nonlinear brain activity in schizophrenia. Hum Brain Mapp 30:403–416

Salvador R, Suckling J, Coleman MR, Pickard JD, Menon D, Bullmore E (2005) Neurophysiological architecture of functional magnetic resonance images of human brain. Cereb Cortex 15:1332–1342

Schindler K, Nyffeler T, Wiest R, Hauf M, Mathis J, Hess CW, Müri R (2008) Theta burst transcranial magnetic stimulation is associated with increased EEG synchronization in the stimulated relative to unstimulated cerebral hemisphere. Neurosci Lett 436:31–34

Schoonheim MM, Geurts JJG, Landi D, Douw L, Van der Meer ML, Vrenken H, Polman CH, Barkhof F, Stam CJ (2011) Functional connectivity changes in multiple sclerosis patients: A graph analytical study of MEG resting state data. Hum Brain Mapp 34:52–61

Shafi MM, Westover MB, Fox MD, Pascual-Leone A (2012) Exploration and modulation of brain network interactions with noninvasive brain stimulation in combination with neuroimaging. Eur J Neurosci 35:805–825

Shu N, Liu Y, Li K, Duan Y, Wang J, Yu C, Dong H, Ye J, He Y (2011) Diffusion tensor tractography reveals disrupted topological efficiency in white matter structural networks in multiple sclerosis. Cereb Cortex 21:2565–2577

Silvanto J, Pascual-Leone A (2008) State-dependency of transcranial magnetic stimulation. Brain Topogr 21:1–10

Silvanto J, Cattaneo Z, Battelli L, Pascual-Leone A (2008) Baseline cortical excitability determines whether TMS disrupts or facilitates behavior. J Neurophysiol 99:2725–2730

Sporns O, Tononi G, Edelman GM (2000) Connectivity and complexity: the relationship between neuroanatomy and brain dynamics. Neural Netw 13:909–922

Srinivasan R, Winter WR, Ding J, Nunez PL (2007) EEG and MEG coherence: measures of functional connectivity at distinct spatial scales of neocortical dynamics. J Neurosci Methods 166:41–52

Stam CJ, Jones BF, Nolte G, Breakspear M, Scheltens P (2007) Small-world networks and functional connectivity in Alzheimer's disease. Cereb Cortex 17:92–99

Stam CJ, De Haan W, Daffertshofer A, Jones BF, Manshanden I, Van Cappellen van Walsum AM, Montez T, Verbunt JPA, De Munck JC, Van Dijk BW, Berendse HW, Scheltens P (2009) Graph theoretical analysis of magnetoencephalographic functional connectivity in Alzheimer's disease. Brain 132:213–224

Stefan K, Gentner R, Zeller D, Dang S, Classen J (2008) Theta-burst stimulation: remote physiological and local behavioral aftereffects. Neuroimage 40:265–274

Strens LHA, Oliviero A, Bloem BR, Gerschlager W, Rothwell JC, Brown P (2002) The effects of subthreshold 1 Hz repetitive TMS on cortico-cortical and interhemispheric coherence. Clin Neurophysiol 113:1279–1285

Thut G, Pascual-Leone A (2010) A review of combined TMS-EEG studies to characterize lasting effects of repetitive TMS and assess their usefulness in cognitive and clinical neuroscience. Brain Topogr 22:219–232

Thut G, Veniero D, Romei V, Miniussi C, Schyns P, Gross J (2011) Rhythmic TMS causes local entrainment of natural oscillatory signatures. Curr Biol 21:1176–1185

Van den Heuvel MP, Mandl RCW, Stam CJ, Kahn RS, Hulshoff Pol HE (2010) Aberrant frontal and temporal complex network structure in schizophrenia: a graph theoretical analysis. J Neurosci 30:15915–15926

Vlachos A, Müller-Dahlhaus F, Rosskopp J, Lenz M, Ziemann U, Deller T (2012) Repetitive magnetic stimulation induces functional and structural plasticity of excitatory postsynapses in mouse organotypic hippocampal slice cultures. J Neurosci 32:17514–17523

Wagner T, Valero-Cabre A, Pascual-Leone A (2007) Noninvasive human brain stimulation. Annu Rev Biomed Eng 9:527–565

Walsh V, Pascual-Leone A (2005) Transcranial magnetic stimulation: a neurochronometrics of mind, new edition. The MIT Press, New York

Watts DJ, Strogatz SH (1998) Collective dynamics of "small-world" networks. Nature 393:440–442

Wheaton LA, Nolte G, Bohlhalter S, Fridman E, Hallett M (2005) Synchronization of parietal and premotor areas during preparation and execution of praxis hand movements. Clin Neurophysiol 116:1382–1390